CHAPTER 2

Structural and Magnetic Characterization of three Tetranuclear Cu(II) complexes with Face-sharing-dicubane / Double-open-cubane like core Framework

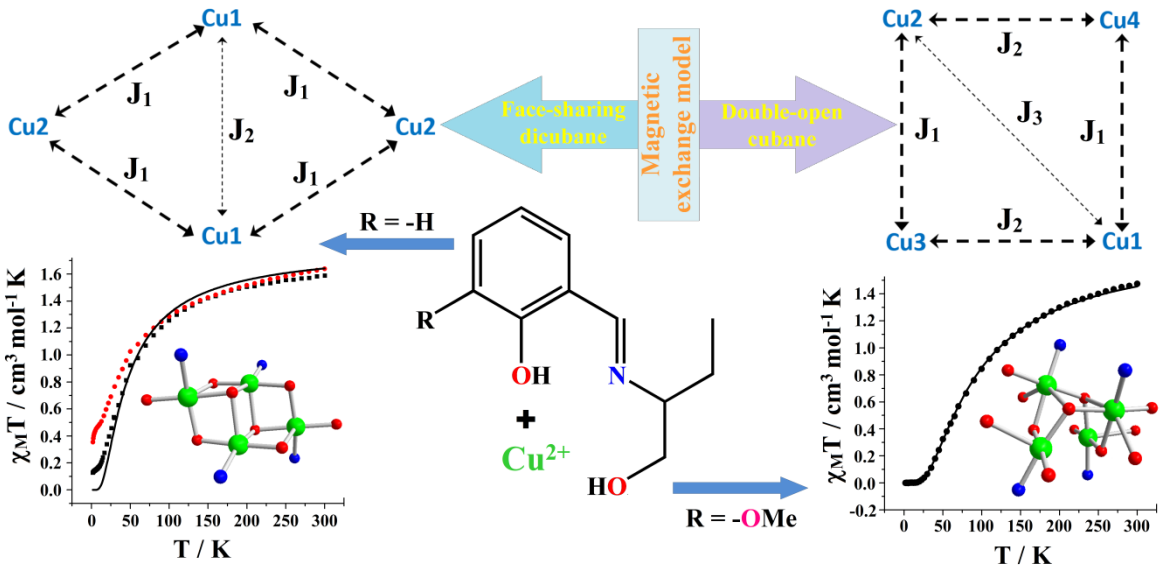

A. Paul et al., *Journal of Solid State Chemistry 249 (2017) 29-38*

2.1 Introduction

High nuclear complexes containing paramagnetic transition metal ions represent important class of compounds for their potential application in the area of molecular magnetism [2.1] and their ability to mimic metalloprotein active sites [2.2]. Among the higher nuclear complexes, tetranuclear copper complexes of various structure e.g. dimeric, [2.3a] square planar [2.3b], cyclic [2.3c], pin-wheel [2.3d], face to face [2.3e], roof-shaped [2.3f] and cubane types [2.3g] are reported in the literature due to their potential application as in the area of magnetism [2.4], catalysis [2.5] and bioinorganic modelling [2.6]. Literature survey reveals that cubane-like copper complexes (Cu_4O_4) containing hydroxo, alkoxo and phenoxo bridges are studied implementing experimental and theoretical approaches with the aim of establishing magneto-structural correlation [2.7]. Depending on the arrangement of the copper and oxygen atoms in Cu_4O_4 units, various cubane geometries such as regular cubane [2.8], single-open cubane [2.9], double open cubane [2.10] and face-sharing dicubane have been reported [2.11].

From the structural point of view two classification for Cu_4O_4 cubane-like complexes have been proposed. Depending on the distribution of the long Cu-O bonds in the cube, Mergehenn and Hasse classified [2.12] the cubanes as type-I and type-II. In the copper cubane where there are four long Cu-O distances between two dinuclear sub-unit categories as type-I. On the contrary when long copper-oxygen distances are within each dinuclear sub-unit are classified as type-II [2.13].

Based on the Cu…Cu distances within the Cu_4O_4 cubane core Alvarez et al. classify [2.14] the copper cubane into three types: (i) (2+4), has two short and four long Cu…Cu distance, which is equivalent to type-I, (ii) (4+2), this class of cubane compound has two long and four short

Cu…Cu distances, and when the Cu_4O_4 core symmetry is S_4, it would be equivalent to type-II, and (iii) (6+0), where six Cu…Cu bonds of Cu_4O_4 cubane core are similar.

Alkoxo and phenoxo donor Schiff bases are potential ligands for the synthesis of cubane compounds. The structure of the cubane core can be tuned by slight modification of Schiff base and reaction conditions [2.15]. In the present contribution we report synthesis, crystal structure and magnetic properties of three tetranuclear copper complexes $[Cu_4(L^1)_4]\cdot 2(dmf)$ (**1**), $[Cu_4(L^1)_4]$ (**2**) and $\{[Cu_4(L^2)_2(HL^2)_2(H_2O)_2]\cdot 2(ClO_4)\cdot 6(H_2O)\}$ (**3**). Complexes **1** and **2** possess face sharing dicubane core structure. On the other hand, complex **3** has double open cubane structure. The different magnetic exchange coupling pathways existing within these compounds have been evaluated by means of variable temperature magnetic measurements and simulations, and the results obtained have been correlated with their corresponding structural features.

2.2 Experimental

2.2.1 Materials and methods

High purity 2-amino-1-butanol (Aldrich Chemical Co. Inc.), 2-hydroxy benzaldehyde and 2-hydroxy-3-methoxybenzaldehyde (Spectrochem-India) were purchased and used as received. All other chemicals used were analytical grade. Solvents used for spectroscopic studies were purifies and dried by standard procedures before use [2.16].

Elemental analyses (C, H and N) were performed using a Perkin-Elmer 240C elemental analyzer. IR spectra were recorded as KBr pellets on a Bruker Vector 22FT IR spectrophotometer operating from 400 to 4000 cm^{-1}. NMR spectra of ligands recorded on Bruker 400 MHz instrument. Electronic absorption spectra were obtained with Shimadzu UV-1601 UV-vis spectrophotometer at room temperature. Quartz cuvettes with a 1 cm path length and a 3 cm^3 volume were used for all measurements.

Temperature-dependent molar susceptibility measurements of polycrystalline sample were carried out at the Servei de Magnetoquímica of the Centres Científics i Tecnològics at the Universitat de Barcelona in a Quantum Design SQUID MPMSXL susceptometer with an applied field of 3000 and 198 G in the temperature ranges 2 - 300 and 2 - 30 K, respectively.

2.2.2 Synthesis of ligands

The ligands (E)-2-((1-hydroxybutan-2-ylimino)methyl)phenol (H_2L^1) and (E)-2-((1-hydroxybutan-2-ylimino)methyl)-6-methoxyphenol (H_2L^2) were prepared by the same general procedure.

H_2L^1. A methanolic solution of 1:1 mixture of 2-aminobutanol and 2-hydroxy benzaldehyde was refluxed for 3 h. The resulting yellow colour solution was cooled to room temperature and solid yellow compound was obtained after evaporation of solvent. Re-crystallization of compound using methanol as solvent resulted yellow crystalline compound. Crystalline solid was collected by filtration and dried in air to afford H_2L^1. Yield: 0.164 g (85%). *Anal.* Calc. for $C_{11}H_{15}NO_2$ (193.24): C, 68.36; H, 7.82; N, 7.24 %. Found: C, 68.34; H, 7.79; N, 7.26 %. ^{1}H NMR (400 MHz, $CDCl_3$, δ ppm): 0.709 - 0.886 (3H, m), 1.474 - 1.655 (2H, m), 2.576 (1H, s), 3.466 - 3.690 (1H, m; 2H, m), 4.957 (1H, s), 6.823 - 6.921 (1H, d; 2H, m), 7.226 - 7.298 (1H, d; 2H, m), 8.306 (1H, s). ^{13}C NMR ($CDCl_3$, 100 MHz, δ ppm): 165.41 (Ar-C-OH), 161.71 (-CH=N-), 132.45 - 113.71 (Ar-C), 73.03 (-CH_2-OH), 66.23 (=N-CH-), 25.05 (-CH_2-), 10.51 (-CH_3).

H_2L^2. Yellow colour ligand was synthesized adopting the same procedure as for H_2L^1, using 2-hydroxy-3-methoxybenzaldehyde instead of using 2-hydroxybenzaldehyde. Yield: 0.187 g (84%). *Anal.* Calc. for $C_{12}H_{17}NO_3$ (223.26): C, 64.49; H, 7.61; N, 6.27 %. Found: C, 64.48; H, 7.63; N, 6.28 %. ^{1}H NMR (400 MHz, $CDCl_3$, δ ppm): 0.900 (3H, m), 1.515 - 1.667 (2H, m),

2.353 (1H, s), 3.169 - 3.208 (1H, m), 3.607 - 3.895 (2H, d; 3H, s), 4.867 (1H, s), 6.689 - 6.941 (1H, d; 2H, m; 1H, d), 8.279 (1H, s). ^{13}C NMR ($CDCl_3$, 100 MHz, δ ppm): 148.70 (Ar-C-OH), 165.46 (-CH=N-), 124.53 - 113.96 (Ar-C), 72.12 (-CH_2-OH), 65.61 (=N-CH-), 56.27 (-O-CH_3), 24.97 (-CH_2-), 10.39 (-CH_3).

2.2.3 Synthesis of complex

Caution! *Perchlorate salts of metal with organic ligands are potentially explosive. Only a small amount of material should be prepared, and it should be handled with care.*

The complexes have been synthesized by adopting the procedures schematically given in Scheme 2.1.

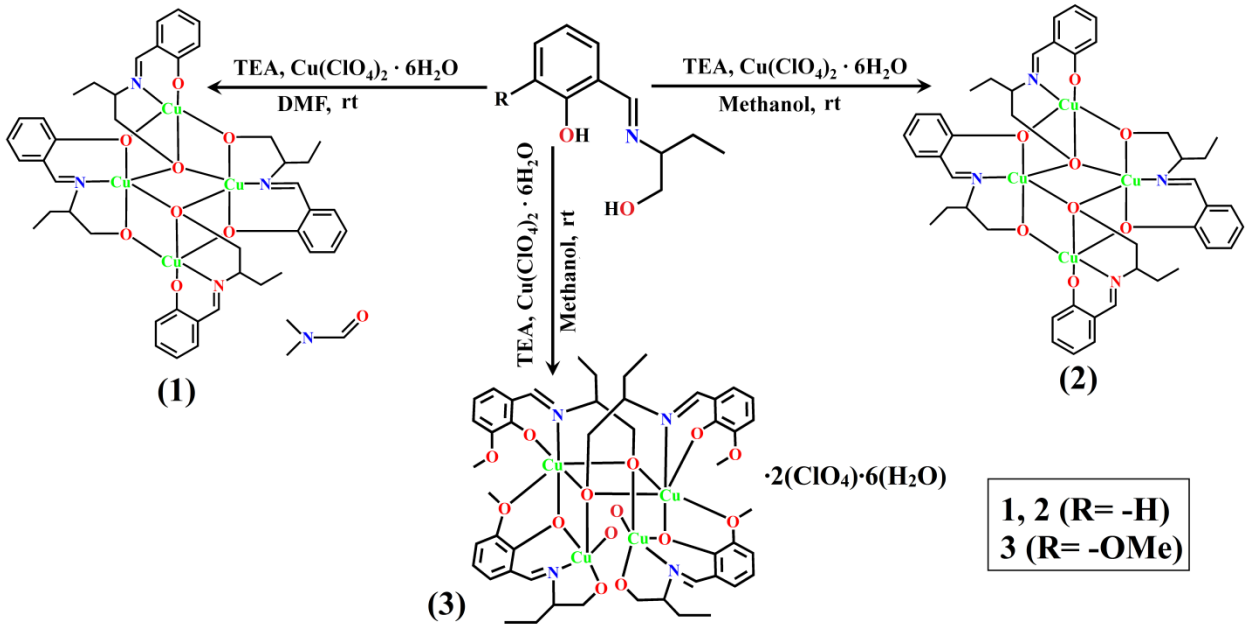

Scheme 2.1. Synthesis of complexes **1-3**.

$[Cu_4(L^1)_4]\cdot 2(dmf)$ (1). A methanolic solution (5 mL) of triethylamine (1 mmol) was added dropwise to a methanolic solution (10 mL) of H_2L^1 (1 mmol, 0.193 g) with constant stirring for 5 min. To this resulting mixture, drop wise addition of DMF solution (15 mL) of copper

perchlorate hexahydrate (1 mmol; 0.370 g) resulted in a deep green solution. The whole reaction mixture was stirred for 2 hours and filtered. The filtrate was kept in air for slow evaporation at room temperature. Green single crystals suitable for X-ray diffraction were obtained after a few days. Yield: 78 %. $C_{50}H_{66}Cu_4N_6O_{10}$ (1165.29): C, 51.53; H, 5.70; N, 7.21 %. Found: C, 50.37; H, 5.54; N, 5.94 (%). IR (cm^{-1}): 2983 (vw), 1641 (vs), 1553 (vs), 1467 (s), 1414 (vs), 1373 (w), 1300 (s), 1246 (vw), 1195 (vw), 1081 (s), 976 (w), 882 (vw), 780 (vw), 740 (vw).

$[Cu_4(L^1)_4]$ (2) and $[Cu_4(L^2)_2(HL)_2(H_2O)_2]\cdot 2(ClO_4)\cdot 6(H_2O)$ (3). Complex **2** was synthesized using same procedure as for complex **1** here only methanol was used as solvent instead of methanol and DMF. Complex **3** was following same procedure as used for complex **1**. Here H_2L^2 (1 mmol, 0.223 g) was used instead of H_2L^1 and only methanol was used as solvent. For **2**: Yield: 81 %. $C_{44}H_{52}Cu_4N_4O_8$ (1019.10): C, 51.85; H, 5.14; N, 5.49 %. Found: C, 51.77; H, 5.69; N, 6.96 (%). IR (cm^{-1}): 2983 (vw), 1646 (vs), 1550 (vs), 1466 (s), 1412 (vs), 1373 (s), 1299 (s), 1244 (vw), 1078 (s), 1012 (vw), 882 (w), 821 (vw).

For **3**: Yield: 77 %. $C_{60}H_{78}Cu_4N_4O_{36}Cl_2$ (1484.20): C, 48.55; H, 5.29; N, 3.77 %. Found: C, 48.51; H, 5.32; N, 3.79 (%). IR (cm^{-1}): 2983 (vw), 1643 (vs), 1550 (vs), 1466 (s), 1414 (vs), 1373 (s), 1299 (s), 1246 (w), 1218 (vw), 1081 (s), 976 (w), 882 (vw), 780 (vw), 740 (vw).

2.2.4. Crystallographic data collection and refinement

Data collection of complexes **1**, **2** and **3** were carried out by using a Nonius Kappa CCD diffractometer with graphite monochromated Mo-Kα radiation, at room temperature. The data sets were integrated with the Denzo-SMN package [2.17] and corrected for Lorentz, polarization and absorption effects (SORTAV) [2.18]. The structures were solved by direct methods using SIR97 [2.19] system of programs and refined using full-matrix least-squares with all non-hydrogen atoms anisotropically and hydrogens included on calculated positions, riding on their

carrier atoms. All calculations were performed using SHELXL-97 [2.20] and PARST [2.21] implemented in WINGX [2.22] system of programs. Graphical programs used are those included in the WINGX System [2.22], and Diamond [2.23]. Crystal data and details of refinements are given in Table 2.1. The cif file CCDC numbers are 1476822- 1476824 for complex **1**-**3**, respectively.

Table 2.1 Crystal data and details of structure refinement of complexes **1** - **3.**

Complex	**1**	**2**	**3**
Empirical formula	$C_{50}H_{66}Cu_4N_6O_{10}$	$C_{44}H_{52}Cu_4N4O_8$	$C_{48}H_{78}C_{l2}Cu_4N_4O_{36}Cl_2$
Formula mass, g mol^{-1}	1165.29	1019.10	1484.20
Crystal system	Monoclinic	Triclinic	Triclinic
Space group	C2/c	P-1	P-1
a, Å	27.1271(4)	8.7510(4)	12.2348(2)
b, Å	10.7513(2)	11.3271(5)	12.9403(2)
c, Å	21.5858(5)	12.3969(6)	22.5308(6)
α, deg	90	105.063(2)	96.1084(7)
β, deg	123.4964(8)	97.907(2)	93.0039(8)
γ, deg	90	106.4407(16)	110.4426(9)
V, $Å^3$	5249.97(18)	1108.12(9)	3308.10(12)
Z	4	1	2
$D_{(calcd)}$, g cm^{-3}	1.474	1.527	1.474
μ(Mo-Kα), mm^{-1}	1.659	1.949	1.431
F(000)	2416	524	1504
Theta range, deg	3.0-30.0	3.0-27.9	3.2-25.0
No. of collected data	19409	13460	27243
No. of unique data	7578	5199	11512
R_{int}	0.043	0.046	0.037
Observed reflns [$I > 2\sigma(I)$]	5519	4047	7076
Goodness of fit (F^2)	1.051	1.027	1.021
Parameters refined	320	272	766
*R*1, *wR*2 ($I > 2\sigma(I)$) [a]	0.0420, 0.1169	0.0475, 0.1522	0.0726, 0.2455
Residuals, e $Å^{-3}$	-0.41, 0.75	-0.61, 0.92	-0.69, 0.65

[a] $R1(Fo) = \Sigma \left| \left| Fo \right| - \left| Fc \right| \right| / \Sigma \left| Fo \right|$, $wR2(Fo^2) = [\Sigma w (Fo^2 - Fc^2)^2 / \Sigma w (Fo^2)^2]^{½}$

2.3 Results and discussion

2.3.1 Synthetic aspects

The multisite coordinating ligands, H_2L^1 and H_2L^2, were prepared by a one pot synthesis employing condensation of the 2-amino-1-butanol and corresponding aldehyde in methanol under reflux condition, and characterized by ^1H and ^{13}C NMR spectra (Figs. 2.1 and 2.2). Using these ligands, complexes **1-3** were synthesized at room temperature.

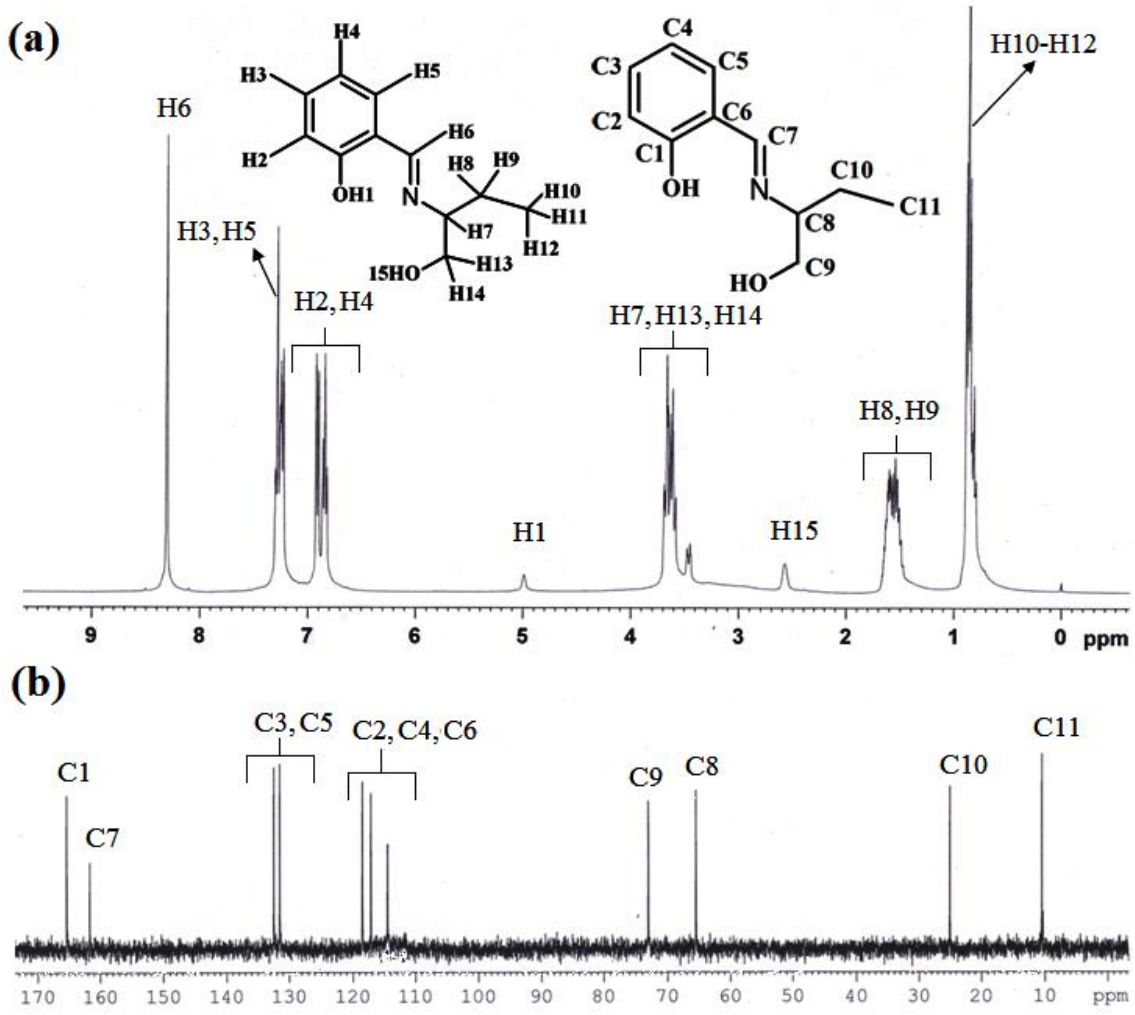

Fig. 2.1 ^1H (**a**) and ^{13}C NMR (**b**) spectra of H_2L^1.

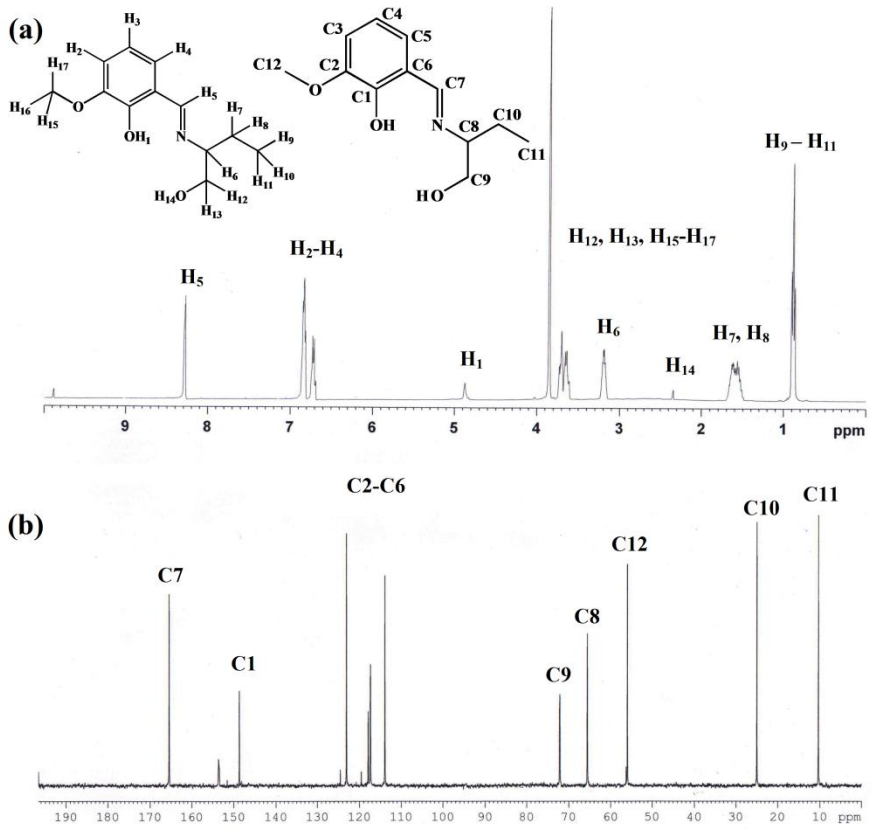

Fig. 2.2 ^{1}H (**a**) and ^{13}C NMR (**b**) spectra of H_2L^2.

2.3.2 Crystal structure description

Complexes [Cu$_4$(L^1)$_4$] ·2(dmf) (1) and [Cu$_4$(L^1)$_4$] (2)

Single crystals of complex **1** were obtained after one week from a saturated methanol-DMF (1:1) solution. On the other hand the single crystals of complex **2** were obtained after a few days by slow evaporation of its saturated methanolic solution. The basic molecular structures of **1** and **2** are shown in Fig. 2.3 and selected bond lengths and angles are listed in Table 2.2.

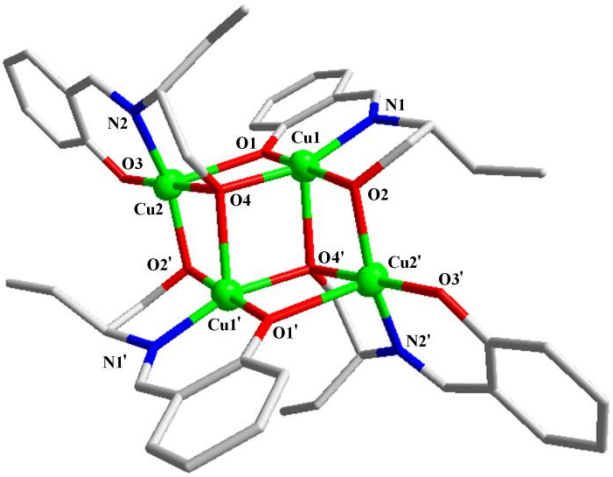

Fig. 2.3 Structure of complex **1** with a partial atom-numbering scheme (Hydrogen atoms are omitted for clarity).

Table 2.2 Coordination bond lengths (Å) and angles (°) for **1** and **2**.

Complex	**1**	**2**
Cu(1)-O(1)	1.918(19)	1.912(3)
Cu(1)-N(1)	1.938(3)	1.917(4)
Cu(1)-O(2)	1.944(16)	1.938(2)
Cu(1)-O(4')	1.978(2)	1.995(2)
Cu(1)-O(4)	2.289(15)	2.258(2)
Cu(2)-O(3)	1.893(19)	1.885(2)
Cu(2)-N(2)	1.953(19)	1.953(4)
Cu(2)-O(4)	1.982(18)	1.969(2)
Cu(2)-O(1')	2.364(2)	2.375(3)
Cu(2)-O(2)	1.9779(15)	1.981(3)
Cu(1)-Cu(2)	3.050(4)	3.025(6)
Cu(1)-O(1)-Cu(2')	93.81(8)	94.17(12)
Cu(1)-O(2)-Cu(2)	102.12(7)	101.10(12)
Cu(1)-O(4)-Cu(2)	90.87(7)	91.16(10)
Cu(1)-O(4)-Cu(1')	98.73(6)	98.99(11)
Cu(1')-O(4)-Cu(2)	104.99(7)	105.50(12)

Complex **1** crystallizes with monoclinic system with C2/c space group, whereas complex **2** crystallizes with triclinic system with P-1 space group. Chemical compositions for both the complexes are same, only difference is the present of one extra lattice DMF in complex **1**. Asymmetric unit of both complexes contain only half of the tetra nuclear unit and second half of the molecule is generated by symmetry transformation. Core structure (Cu_4O_6) of both the

compounds posses face shared dicubane structure (Fig. 2.4), where one corner atom is missing in each cube (Scheme 2.2).

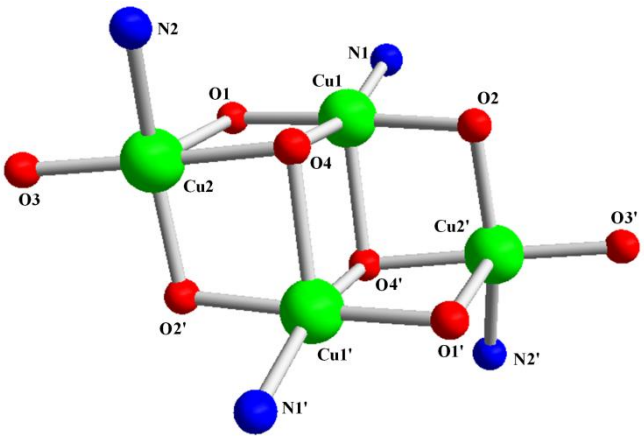

Fig. 2.4 Simplified representation of the coordination environment of the four metal centres in complexes **1** and **2.**

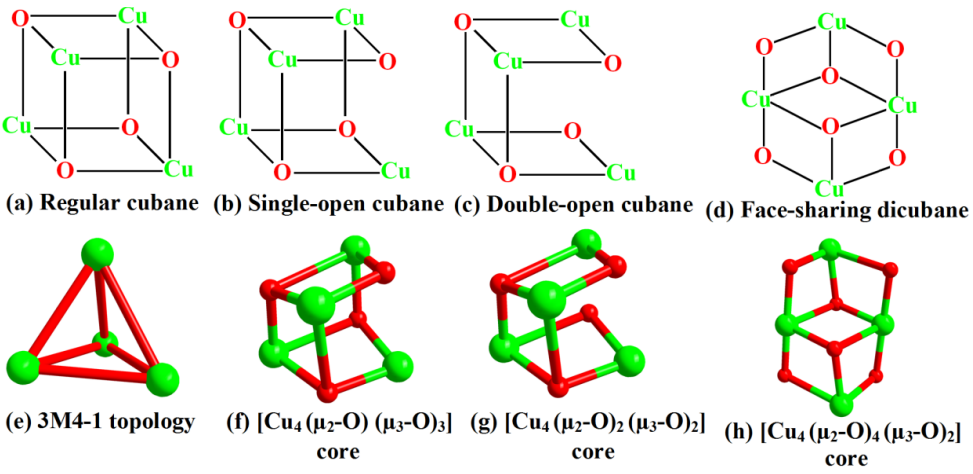

Scheme 2.2. Representation of (a) regular, (b) single open, (c) double open cubane cores (Cu_4O_4) and (d) face-sharing dicubane core (Cu_4O_6) with missing two vertices and (e) Simplified Topological Graph Showing a Uninodal 3-Connected Motif with 3M4-1 Topology in cubane core. Ball-and-Stick Representation of Distorted (f) Single-Open [$Cu_4(\mu_2\text{-}O)(\mu_3\text{-}O)_3$], (g) Double-Open [$Cu_4(\mu_2\text{-}O)_2(\mu3\text{-}O)_2$] Cubane Cores and (h) Face-sharing dicubane [$Cu_4(\mu_2\text{-}O)_4(\mu_3\text{-}O)_2$] with two missing vertices. Color code: Cu centers, green balls; O atoms, red balls.

The tetra-nuclear dicubane complex consists of four di-deprotonated ligands [$(L^1)^{2-}$] and each of them coordinate with copper atom with N, O, O donor centers. The Cu_4O_6 core structure was

formed by the two μ_3-O, four μ_2-O bridging with peripheral supports from four μ_1-N and two μ_1-O in a centrosymmetric arrangement. Copper centers possesses two types of distorted square pyramidal coordination arrangement [τ = 0.187 and 0.377 for Cu1 and Cu2, respectively for **1;** τ = 0.257 and 0.328 for Cu1 and Cu2, respectively for **2**]. Cu1 and Cu1' are bridged with two bridging μ_3-alkoxide oxygen atoms (O4 and O4') and other coordination sites are fulfilled with μ_2-phenoxo bridge oxygen (O1 and O1'), μ_2-alkoxo oxygen (O2 and O2') and imine nitrogen atoms (N1 and N1'). Coordination environment of Cu2 centre is completed by μ_3-alkoxo (O4), μ_2-alkoxo (O2), μ_2-phenoxo (O1), μ_1-phenoxo (O3) and μ_1-N imine (N2) nitrogen atoms. The Cu-Cu distances in five faces of the dicubane are ranges 3.050 Å - 5.275 Å for **1,** whereas 3.026 Å - 5.267 Å for **2**. The coordination Cu-O bond distances are varying in the range 1.893(19) Å - 2.364(2) Å for **1** and 1.885(2) Å - 2.375(3) Å for **2**. On the other hand the Cu-N separation varies in the range 1.938(3) Å - 1.953(2) Å and 1.917(4) Å - 1.953(4) Å for **1** and **2** respectively. The bond angles between the successive coordinating equatorial atoms of Cu1 centre are 85.78(8), 95.44(7), 85.20(9) and 93.74(9)° (for **1**) and 85.49(11), 96.36(10), 85.10(13) and 94.26(13)° (for **2**), where the first angle is O(1)-Cu(1)-O(4) and the last one is N(1)-Cu(1)-O(1) for both the complexes whereas the angles between the axial atom, Cu1 and equatorial atoms are 100.35(7), 81.27(7), 79.29 (6) and 111.16(8)° (for **1**) and 95.00(10), 86.61(10), 83.75(13) and 94.08(13)° (for **2**). In Cu2 centre the bond angles between the successive coordinating equatorial atoms with Cu2 are 86.51(6), 95.27(7), 83.56(8) and 94.55(8)° (for **1**) and 81.01(10), 96.95(11), 80.03(10) and 118.08(14)° (for **2**). The angles between the axial atom, Cu2 and equatorial atoms are 101.98(9), 96.87(7), 74.61(7) and 105.75(8)° for **1** and 107.11(10), 94.45(10), 74.62(10) and 102.17(13)° for **2** respectively. Packing diagram of **1** shows that it possess as a 2D layer (Fig.

2.5) structure which was formed with three different types of C-H...π interactions [2.24] [C-H...Cg = 2.680 Å, 3.162 Å and 3.258 Å] (Table 2.3).

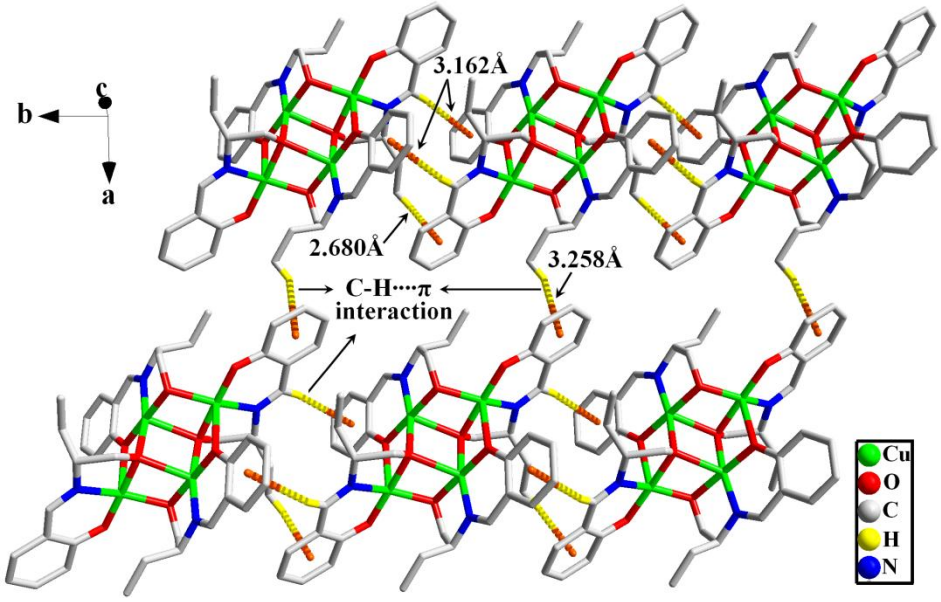

Fig. 2.5 2D supramoleular structure of complex **1** formed with C-H...π interactions.

Table 2.3 C-H…π interactions in complexes **1** and **2.**

C-H	Cg(J)	H···Cg (Å)	X-H···Cg (°)	X···Cg (Å)
*Complex **1***				
C(22)-H(22B)	Cg(18)→ C(12) - C(13)- C(14) - C(15) -C(16) - C(17)	2.680	161.00	3.603(4)
C(18)-H(18)	Cg(17)→ C(1) - C(2)- C(3) - C(4) -C(5) - C(6)	3.162	166.71	4.072
C(11)-H(11A)	Cg(18)→ C(12) - C(13)- C(14) - C(15) -C(16) - C(17)	3.258	132.36	3.968
*Complex **2***				
C(15)-H(15)	Cg(18)→ C(1) - C(2)- C(3) - C(4) -C(5) - C(6)	3.164	144.95	3.961
C(10B)-H(10D)	Cg(19)→ C(12) - C(13)- C(14) - C(15) -C(16) - C(17)	3.187	128.52	3.867

Tetrameric units are connected through two C-H...π interactions (C-H...Cg = 2.680Å; 3.162Å) and form 1D supramolecular chain. The 1D chains are again interconnected through another type C-H...π interaction (C-H...Cg = 3.258Å) and results 2D supramolecular structure. On the other hand packing diagram of **2** indicates that it exist as a 2D layer (Fig. 2.6) through two different types of C-H...π interactions [C-H...Cg = 3.164 Å and 3.187 Å] and one type π...π stacking interaction [2.25] [Cg...Cg = 4.020Å].

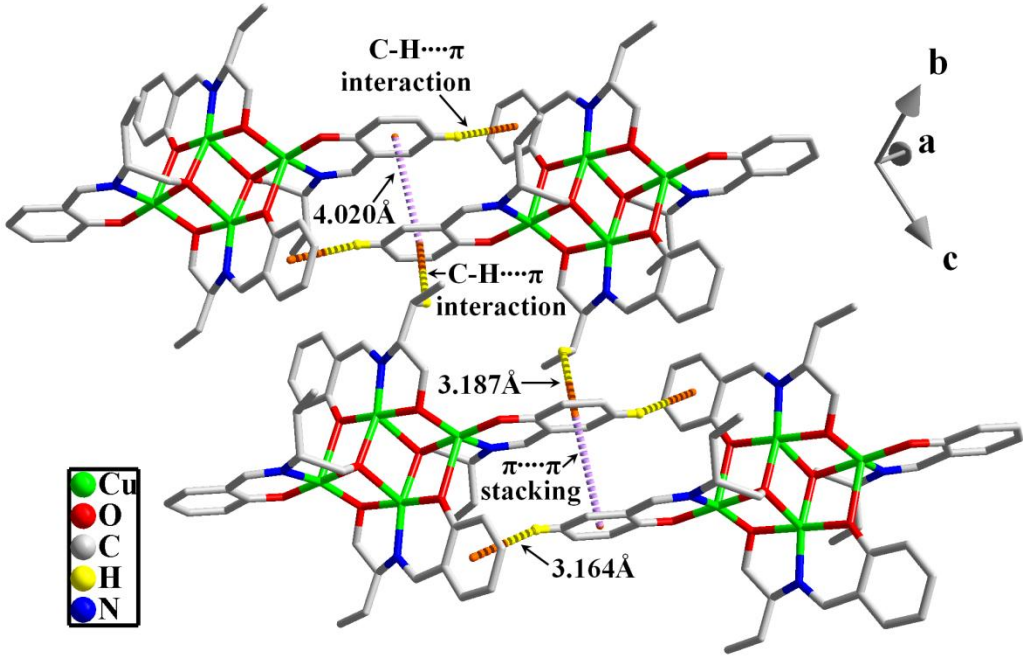

Fig. 2.6 2D supramoleular structure of complex **2** formed with C-H...π and π...π interactions.

Here tetrameric units are connected through C-H...π (C-H...Cg = 3.164 Å) and π...π interactions (Cg...Cg = 4.020 Å) to form 1D supramolecular chain, and these 1D chains are again connected through other C-H...π interaction (C-H...Cg = 3.187 Å) and finally result 2D supramolecular structure.

Complex {[$Cu_4(L^2)_2(HL^2)_2(H_2O)_2$]·2($ClO_4$)·6($H_2O$)} (3)

The molecular structures of complex **3** are shown in Figs. 7 and 8. The compound crystallizes with triclinic crystal system and P-1 space group. The core symmetry of complex **3** possesses double-open cubane structure (Scheme 2.2). The complex contain four copper(II) centres, two dideprotonated ligands [$(L^2)^{2-}$], two monodeprotonated ligands [$(HL^2)^-$] and two coordinated water molecules.

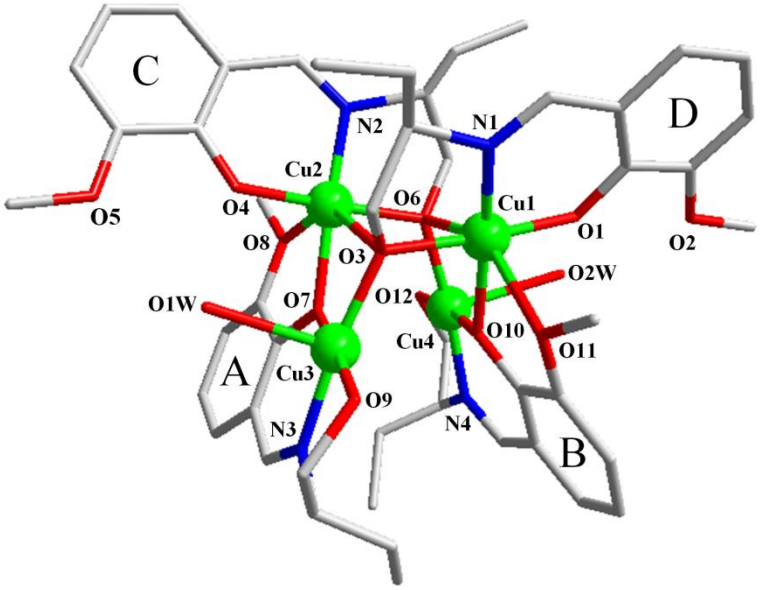

Fig. 2.7 Structure of complex **3** with a partial atom-numbering scheme (Hydrogen atoms are omitted for clarity).

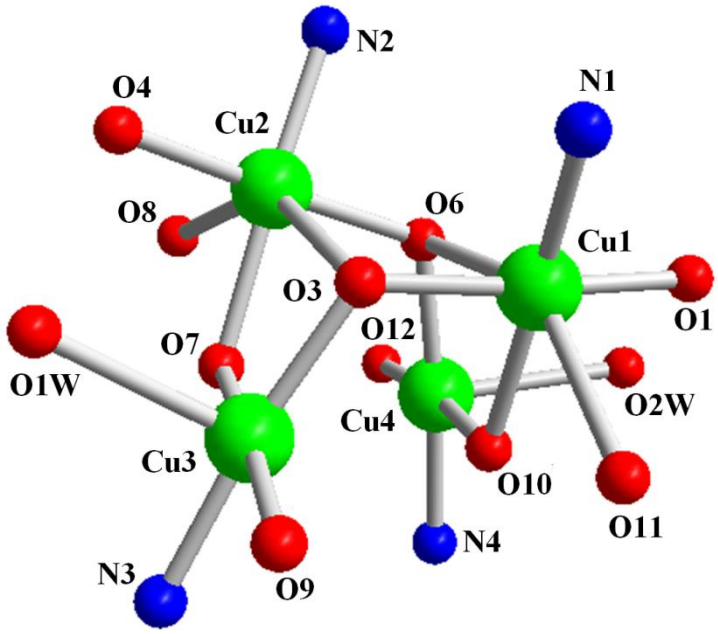

Fig. 2.8 Simplified representation of the coordination environment of the four metal centres in complex **3**.

Each mono deprotonated ligand (A and B rings in Fig. 2.7) chelates two copper atoms *via* μ_2-η^1:η^1:η^1:η^2-*O,O,N,O* coordination mode, while the double deprotonated ligand (C and D rings in Fig. 2.7) chelates Cu1 and Cu2 centres, and in addition connect the previous moieties with the μ_3-alkoxido group, while the methoxy oxygen O2 and O5 are remain uncoordinated (μ_3-η^1:η^1:η^3-*O,N,O* coordination mode). The pair of ligands A/B and C/D are arranged in a head-tail fashion about the cubane-like core so that the complex presents a pseudo two-fold axis passing in between Cu3/Cu4 and Cu2/Cu1. Fig. 2.8 shows a simplified representation of the coordination environment around the four copper centers. The metal ions Cu3 and Cu4 present a similar distorted square pyramidal geometry (τ = 0.046 and 0.021 for Cu3 and Cu4 respectively). The basal plane of the square pyramid formed by the imine nitrogen, the phenoxide oxygen and the alcoholic oxygen of mono deprotonated ligands [$(HL^2)^-$] and μ_3-alkoxido oxygen of double deprotonated ligand [$(L^2)^{2-}$]. The coordinated water molecule occupied the apical position of the square pyramid. The basal coordination bond lengths for Cu3 and Cu4 are in between 1.911(5) - 2.005(7) Å. The bond lengths between oxygen atom of water ligand and copper are somewhat more distant, being at 2.398(7) and 2.428(7) Å for Cu3 and Cu4 respectively (Table 2.4). The bond angles between the successive coordinating equatorial atoms with Cu3 atom are 87.22(2)°, 96.95(2)°, 82.67(3)° and 93.04(2)° and the angles between the axial atom, Cu3 and equatorial atoms are 89.63(2)°, 94.23(2)°, 91.28(2)° and 92.82(2)° whereas in Cu4 the bond angles between the successive coordinating equatorial atoms with Cu4 are 87.74(19)°, 97.49(2)°, 81.53(3)° and 92.89(2)° and the angles between the axial atom, Cu4 and equatorial atoms are 92.09(2)°, 93.56(2)°, 91.63(2)° and 91.63(3)°.

Table 2.4 Coordination bond lengths (Å) and angles (°) for **3**.

Cu(1)-O(1)	1.892(6)	Cu(2)-O(3)	2.476(5)
Cu(1)-N(1)	1.930(5)	Cu(3)-N(3)	1.934(6)
Cu(1)-O(3)	1.953(5)	Cu(3)-O(7)	1.951(5)
Cu(1)-O(10)	2.024(4)	Cu(3)-O(9)	1.999(7)
Cu(1)-O(11)	2.392(5)	Cu(3)-O(3)	1.911(5)
Cu(1) -O(6)	2.492(5)	Cu(3)-O(1W)	2.398(7)
Cu(2)-O(4)	1.897(6)	Cu(4)-O(10)	1.938(5)
Cu(2)-N(2)	1.920(7)	Cu(4)-N(4)	1.934(6)
Cu(2)-O(6)	1.952(5)	Cu(4)-O(6)	1.921(5)
Cu(2)-O(7)	2.021(5)	Cu(4)-O(12)	2.005(7)
Cu(2)-O(8)	2.419(5)	Cu(4)-O(2W)	2.428(7)
Cu(1)-O(3)-Cu(3)	118.8(3)	Cu(3)-O(7)-Cu(4)	104.18(18)
Cu(1)-O(3)-Cu(2)	94.8(2)	Cu(2)-O(7)-Cu(3)	106.0(2)
Cu(2)-O(3)-Cu(3)	91.73(18)	Cu(2)-O(7)-Cu(4)	83.82(17)
Cu(1)-O(6)-Cu(2)	94.3(2)	Cu(3)-O(10)-Cu(4)	103.47(17)
Cu(1)-O(6)-Cu(4)	91.14(18)	Cu(1)-O(10)-Cu(3)	83.01(15)
Cu(2)-O(6)-Cu(4)	118.3(2)	Cu(1)-O(10)-Cu(4)	106.59(19)

The coordination environment of Cu1 and Cu2 are also similar, both the metal centre remains in distorted octahedral geometry. The basal plane of the octahedron formed by the imine nitrogen, the phenoxido and the alkoxido oxygen from one $(L^2)^{2-}$ ligand and μ_2-phenoxido oxygen of $(HL^2)^-$, the axial positions are the occupied by methoxy oxygen of same $(HL^2)^-$ and the alkoxido oxygen atom of another $(L^2)^{2-}$ ligand. The equatorial bond distances are in the range 1.892(6) - 2.024(4) Å, while the axial bond lengths vary from 2.392(5) to 2.492(5) Å due to the Jahn-Teller distortion. The Cu(3) - O(10) and Cu(4)-O(7) distances are long of 2.896(5) and 2.866(5) Å respectively, responsible for the double open cubane core. The copper atoms are located at the vertices of a distorted tetrahedron (Fig. 2.9) with edge dimension ranges between 3.173 to 3.325 Å, but the Cu3-Cu4 distance of 3.842 Å is the longest.

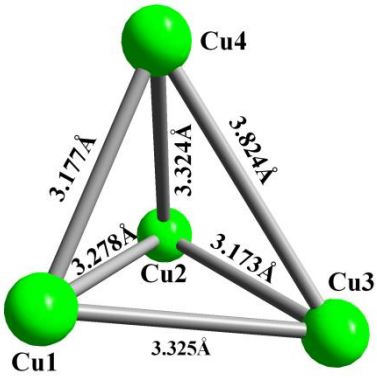

Fig. 2.9 Arrangement of four copper atoms of complex **3** in a distorted tetrahedron.

For the Cu1 and Cu2 the trans angles are in between 71.78(17)° to 115.65(2)° and the cis angles ranges between 84.74(2)° to 94.72(2)°. Based on Cu...Cu distance, Cu_4O_4 core have been classified as (i) (2+4), where Cu...Cu distances are two short and four long; (ii) (4+2) where Cu...Cu distances are two long and four short; and (iii) (6+0), all Cu...Cu distances are identical [2.14c]. In the core structure of complex **3** four Cu...Cu distances are short and two are long and hence core Cu_4O_4 of **3** can be classified as (4+2) system (Scheme 2.3). To get better understanding about the structures of **1-3**, comparisons with the reported similar structures are given in Table 2.5.

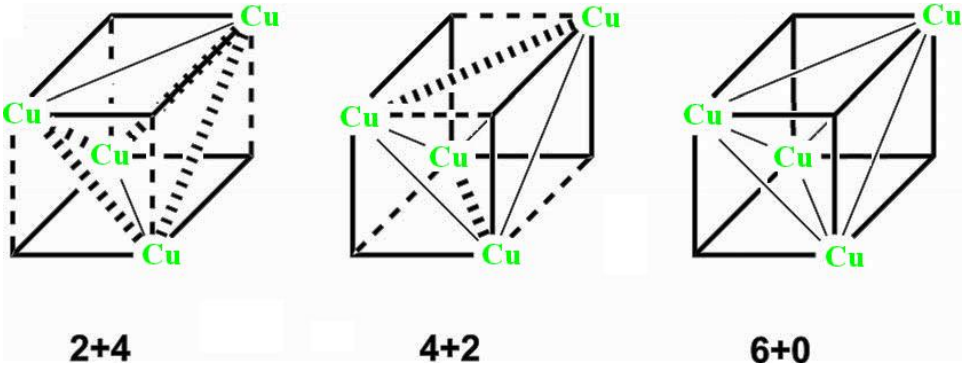

Scheme 2.3. Schematic drawing of the three types of cubane complexes according to the Cu-O and Cu···Cu distances of the central Cu_4O_4 core. Short Cu···Cu distances (solid lines), long Cu···Cu distances (hashed lines), short Cu–O bond lengths (bold lines), and long Cu–O distances (dashed lines).

Table 2.5 Tetranuclear copper complexes with cubane-core.

Complex	Crystal system	Space group	Class	α(Cu–O–Cu)/°	Cu–O short distance (Å)	Cu–O long distance (Å)	d_2(Cu···Cu) [Å]	Ref.
$[Cu_4(L^1)_4]\cdot$(DMF)	Monoclinic	C2/c	-	90.87- 104.99	1.893	2.364	3.050-5.275	This work
$[Cu_4(L^1)_4]$	Triclinic	P-1	-	91.16- 105.50	1.885	2.375	3.026-5.267	This work
$\{[Cu_4(L^2)_2(HL^2)_2(H_2O)_2]\cdot 2(ClO_4)\cdot 6(H_2O)\}$	Triclinic	P-1	4+2	83.01-118.8	1.892	2.492	3.173-3.842	This work
$[\{Cu(H_2L^3)\}_4]$	Monoclinic	$P2_1/c$	4+2	88.45-107.97	1.868	1.968	3.114-3.378	[2.13]
$[\{Cu(H_2L^4)\}_4]$	Triclinic	*P*-1	4+2	89.95-109.50	1.890	1.999	3.058-3.384	[2.13]
$[Cu_4(L^5)_2(HL^5)_2(H_2O)]\ (ClO_4)_2\cdot 2H_2O$	Monoclinic	P21/n	4+2	106.1-119.8	1.956	2.001	3.351-3.752	[2.26]
$[Cu_4(NSI)_4].\ 2C_2H_5OH\cdot 2H_2O$	Monoclinic	P2(1)	4+2	108.7-110.9	1.927	1.972	3.176-3.531	[2.27]
$[Cu_4L^6_4]\cdot 5CH_3OH\cdot H_2O$	Triclinic	*P*-1	4+2	102.0-109.4	1.886	1.984	3.095-3.413	[2.28]
$[Cu_4L_4^7]\cdot 2H_2O$	Orthorhombic	*Pbcn*	4+2	101.3-106.1	1.951	1.973	3.06-3.48	[2.29]
$[Cu_4(hsae)_4]\cdot 2H_2O\cdot 4CH_3CN$	Monoclinic	C2/c	4+2	104.8-106.1	1.894	1.956	3.108-3.615	[2.30]
l-$[Cu_4(Hvap)_2(vap)_2(MeOH)_2](NO_3)_2\cdot$ MeOH	Monoclinic	$P2_1$	4+2	90.24-127.66	1.933	1.991	3.152- 4.059	[2.31]
$[Cu_4(H_2L^8)_4]\cdot 10H_2O$	Tetragonal	I4(1)/a	4+2	89.45- 106.70	1.962	1.967	3.152-3.417	[2.32]
$[Cu_4(HL^9)_4]$	Monoclinic	C2/c	-	1.90-1.92	1.900	1.920	3.40-3.45	[2.33]
$[Cu_4(HL^9)_4]\cdot$ 3.5 MeOH·2.25 H_2O	Monoclinic	P21/c	-	86.6-116.0	1.873	1.978	3.116-3.533	[2.33]
$[Cu_4(L^{10})_4]\cdot$2.4(acetone)	Tetragonal	I41/a	4+2	90.8-104.0	1.908	2.362	3.09-3.31	[2.7b]
$[Cu_4(L^{11})_4]$	Monoclinic	C2/c	4+2	90.10-107.6	1.91	2.43	3.12-3.38	[2.7b]
$[Cu_4(L^{12})_4]\cdot$6(toluene)	Orthorhombic	Fdd2	6+0	92.1-108.0	1.909	2.406	3.14-3.24	[2.7b]
$[Cu_4(L^{13})_4]\cdot 4(C_4H_8O_2)$	Tetragonal	I41/a	4+2	90.8-108.9	1.881	2.395	3.11-3.17	[2.34]
$[\{Cu(L^{14})\}_4]$	Orthorhombic	$P2_12_12_1$	2+4	89.79-104.55	1.891	2.566	2.815-3.505	[2.35]
$[(L^{15})_4Cu_4(OH)_4](ClO_4)_4\cdot H_2O$	Monoclinic	C2/c	4+2	91.75-103.30	1.950	2.326	3.081-3.345	[2.36]
$[Cu_4(\mu_4\text{-}H_2edte)(\mu_5\text{-}H_2edte)(sal)_2]n\cdot 10nH_2O$	Orthorhombic	Pbca	-	-	1.890	2.90	3.129-3.624	[2.9]
$[Cu_4(\mu_4\text{-}Hedte)_2(Hpmal)_2(H_2O)]\cdot 7.5H_2O$	Triclinic	P-1	-	-	1.917	2.576	3.102-3.548	[2.9]
$[Cu_4(L^{16})_4]$.(NMP)	Monoclinic	C2/c	-	-	1.885	2.301	3.05-5.237	[2.11b]

H_2L^1: (E)-2-((1-hydroxybutan-2-ylimino)methyl)phenol, H_2L^2: (E)-2-((1-hydroxybutan-2-ylimino)methyl)-6-methoxyphenol, H_2L^3 : *N*-(2-hydroxyethyl)-3,5-di*tert*-butylsalicylaldimine, H_2L^4 : *N*-(2-hydroxyethyl)-4-methoxysalicylaldimine, H_2L^5: 2-[(2-hydroxy-ethylimino)-methyl]-6-methoxy-phenol, H_2L^6 : 2-(5-fluorosalicylideneamino)ethanol, H_2L^7 : 4-chloro-2-[(*E*)-(2-hydroxyethylimino)methyl]phenol, H_2L^8 : tris(hydroxymethyl)(2-hydroxybenzylamino)methane, H_2L^9 : 2-(β-naphthalideneamino)-2-(hydroxymethyl)-1-propanol, $L^{10}H_2$: 1,1,1-trifluoro-7-hydroxy-4-phenyl-5-azahept-3-en-2-one, $L^{11}H_2$: 1,1,1-trifluoro-7-hydroxy-4-phenyldiazenyl -5-azahept-3-en-2-one, $L^{12}H_2$: 1,1,1-trifluoro-7-hydroxy-4- anthracenyl -5-azahept-3-en-2-one, L^{13}H2: A tridentate enaminone, L^{14}H2: benzyl 2-deoxy-2-salicylideneamino-R-D-glucopyranoside, L^{15}: N-benzyl-1-(2-pyridyl)methaneimine, L^{16} H2: salicylidene-2-aminobenzoic alcohol, NSI: hydroxethylsalicydeneimine, H_2hase : (2-(4-hydroxysalicylideneamino)ethanol, l-H_2vap: derived from the condensation of o-vanillin and l-2-amino-3-phenyl-1-propanol, H4edte: N,N,N′,N′-tetrakis(2-hydroxyethyl)ethylenediamine, H_2sal: Salicylic acid , H_2pma: phenylmalonic acid, NMP: N-methylpyrrole.

2.3.3 Electronic absorption spectra of complexes 1-3

The electronic spectra of complexes **1**, **2** and **3** were recorded in methanol and are shown in Fig. 2.10. The spectrum of **1** shows a significant transition at 217 nm ($\varepsilon \sim 9.8 \times 10^4$ liter mole^{-1} cm^{-1}), 237 nm ($\varepsilon \sim 1.8 \times 10^4$ liter mole^{-1} cm^{-1}), 265 nm ($\varepsilon \sim 1.04 \times 10^4$ liter mole^{-1} cm^{-1}), and 355 nm ($\varepsilon \sim 3.6 \times 10^3$ liter mole^{-1} cm^{-1}). Complex **2** shows a significant transitions at 217 nm ($\varepsilon \sim 5.1 \times 10^4$ liter mole^{-1} cm^{-1}), 237 nm ($\varepsilon \sim 5.06 \times 10^4$ liter mole^{-1} cm^{-1}), 266 nm ($\varepsilon \sim 2.86 \times 10^4$ liter mole^{-1} cm^{-1}) and 355 nm ($\varepsilon \sim 1.06 \times 10^4$ liter mole^{-1} cm^{-1}). On the other hand the electronic spectrum of complex for **3**, shows three significant transitions are at 232 nm ($\varepsilon \sim 2.69 \times 10^5$ liter mole^{-1} cm^{-1}), 274 nm ($\varepsilon \sim 1.31 \times 10^5$ liter mole^{-1} cm^{-1}), and 369 nm ($\varepsilon \sim 2.68 \times 10^4$ liter mole^{-1} cm^{-1}).

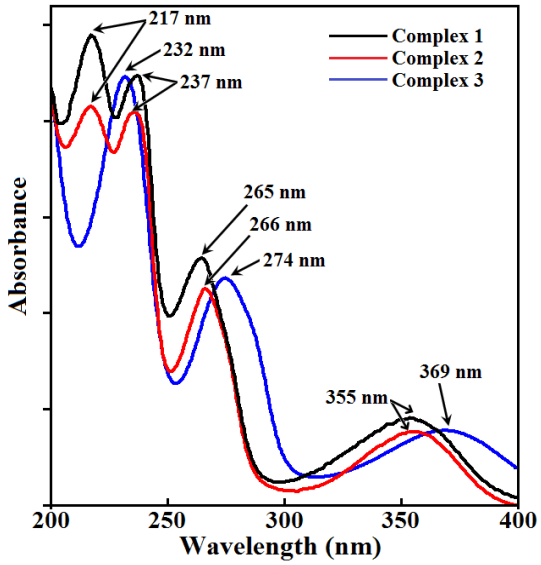

Fig. 2.10 Electronic absorption spectra of complexes **1**, **2** and **3**.

2.3.4 Magnetic properties of complexes

Temperature-dependent magnetic susceptibility measurements on polycrystalline samples of complexes **1** - **3** were carried out in the temperature range 1.9 - 300 K. The plot of $\chi_M T$ versus T for complexes **1** and **2** is shown in Fig. 2.11, where χ_M is the molar magnetic susceptibility and T is the absolute temperature. The $\chi_M T$ value measured at room temperature of 1.58 and 1.64 cm^3 K mol^{-1} is slightly higher than the expected value for four uncoupled S = ½ spins assuming g = 2 (1.48 cm^3 K mol^{-1}). Upon cooling, $\chi_M T$ varies smoothly and finally decreases abruptly below 100 K. At temperatures below 15 K both complexes show a decrease of thr slope of the curve, evidencing a significantly smoother variation of the $\chi_M T$ value with temperature. Nevertheless the $\chi_M T$ vs T curve drops further abruptly at very low temperature again.

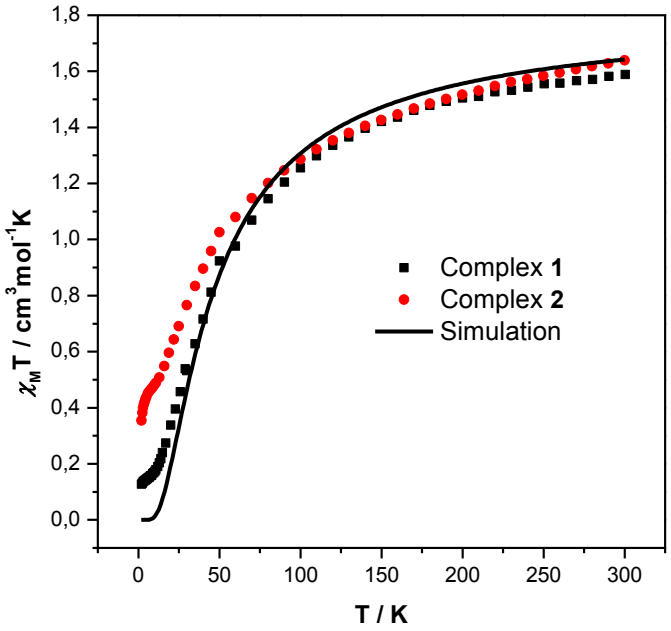

Fig. 2.11 Thermal dependence of the $\chi_M T$ for complexes **1** and **2**. The solid line is a simulation considering the magnetic model shown in Fig.12B for the Type B face-sharing dicubane structure characteristic of complexes **1** and **2**, using the parameters mentioned in the text. The presence of impurities was not considered in the simulation.

The behaviour displayed by complexes **1** and **2** confirms the presence of an overall antiferromagnetic interaction. The vertex-defective face-sharing dicubane structure showed by both complexes is characterized by a Cu_4O_6 core as the one in Fig. 2.12A. In such structure, each Cu(II) ion adopts a square pyramidal geometry, where four coordinating atoms define the equatorial plane characterized by short bond lengths, and a fifth coordinating atom defines the long axial position. The unpaired electron in each Cu(II) ion resides mainly in the basal $d_{x^2-y^2}$ orbital. Thus, those Cu-Cu pairs involving the equatorial planes of the two Cu(II) ions in the bridging pathway are expected to show a significant antiferromagnetic exchange due to effective overlap of magnetic orbitals through the μ_2- or μ_3-O ligand. On the contrary, a weak

ferromagnetic or null exchange coupling will be most likely observed in those Cu-Cu pairs where the magnetic exchange is mediated by an equatorial $d_{x^2-y^2}$ magnetic orbital of one of the Cu(II) ions and an axial d_{z^2} non-magnetic orbital of the other Cu(II) ion.

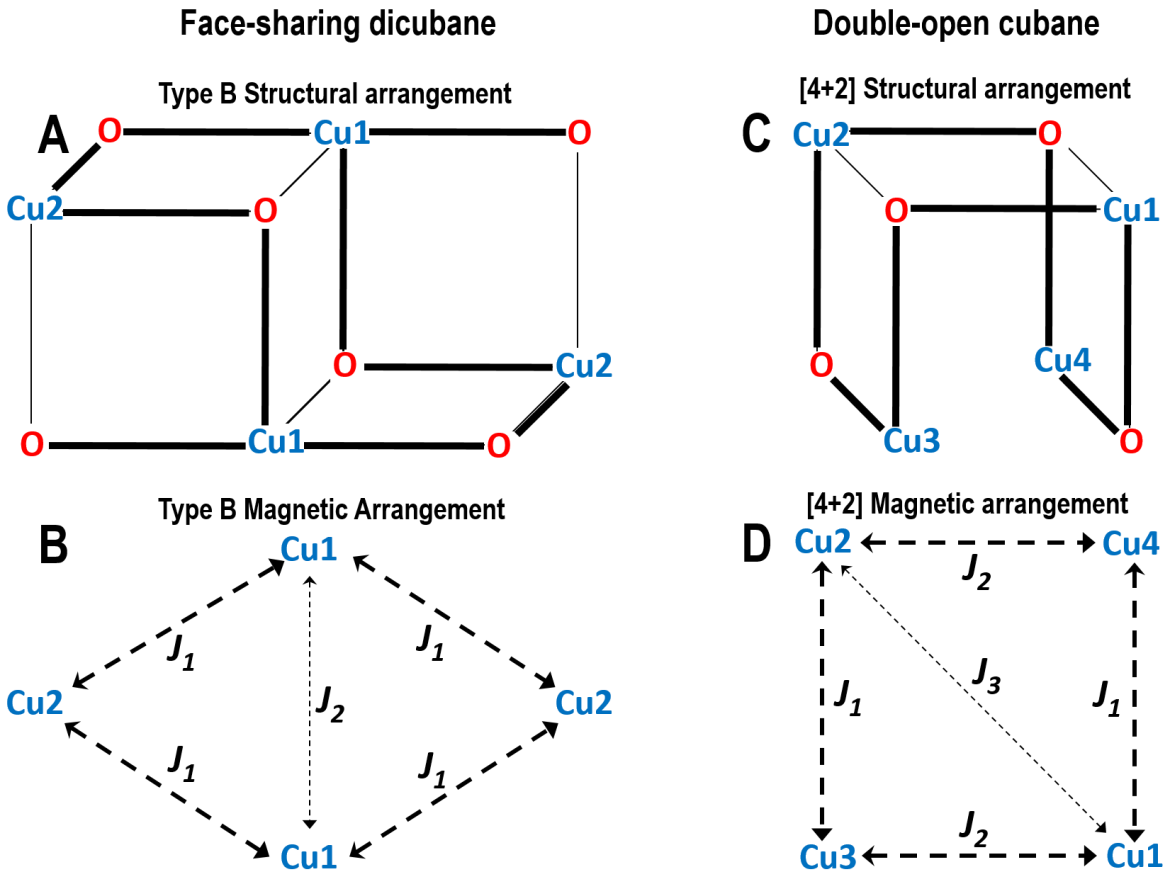

Fig. 2.12 A) Structural arrangement of a type B vertex-defective face-sharing dicubane structure like the one of complexes **1** and **2**, where short (equatorial) and long (axial) Cu-O bonds have been illustrated with thick and thin lines, respectively. B) Magnetic model used for the description of structures like those represented in A. C) Structural arrangement of a [4+2] double-open cubane structure like complex **3**, where short (equatorial) and long (axial) Cu-O bonds have been illustrated with thick and thin lines, respectively. D) Magnetic model used for the description of structures like those represented in C.

Depending on the dihedral angles between neighbouring equatorial planes, face-sharing dicubane structures could be classified into two types. Type A dicubane structures can be structurally and magnetically regarded as a dimer-of-dimers, where intradimer Cu-Cu bridging pathways are all

exclusively based on short equatorial Cu-O bonds and consequently large antiferromagnetic exchange constants might be observed. On the other hand, interdimer Cu-Cu bridging pathways do all involve long axial Cu-O bonds and as a result very weak or null magnetic exchange couplings are established [2.37]. On the contrary, in type B dicubane structures like the one depicted in Fig. 2.12A, each Cu1-Cu2 pair shows two bridging pathways involving equatorial-equatorial and equatorial-axial bridging modes, while Cu1-Cu1' pairs contain only equatorial-axial bridging pathways. Thus, all Cu1-Cu2 magnetic interactions (J_1) become equivalent and are expected to be weakly antiferromagnetic, although significantly stronger than Cu1-Cu1' interactions (J_2) [2.38]. Complexes **1** and **2** of the present work belong to the type B face-sharing dicubane structure.

Considering the structural similarities showed by the Cu_4O_6 cores in complexes **1** and **2**, the magnetic structure can be considered analogous and the exchange model showed in Fig. 2.12B can be used to describe the magnetic behaviour of the two systems. The PHI program was used to study their magnetic behaviour [2.39]. The Hamiltonian used is expressed as $H = -J_1(S_1S_2+S_1S_{2'}+S_{1'}S_2+S_{1'}S_{2'}) - J_2S_1S_{1'}$, where $S_1 = S_{1'} = S_2 = S_{2'} = S_{Cu} = 1/2$, and where the Cu2-Cu2' interaction was considered negligible due to the long distance between paramagnetic centers. Assuming an antiferromagnetic exchange between Cu1 and Cu2 ions ($J_1 < 0$) and considering $|J_1| >> |J_2|$, in agreement with previously discussed magneto-structural issues, then a continuous decrease of $\chi_M T$ with decreasing temperature should be expected, reaching or approaching 0 at low temperatures as a result of an S = 0 ground state, as show in the simulation depicted in Fig. 2.11, where the following values were used: $g_1 = g_2 = 2.20$; $J_1 = -20$ $cm^{-1}$and $J_2 = 0$ cm^{-1}. Nevertheless, the $\chi_M T$ vs T curves for complexes **1** and **2** only display the formation of pseudo-plateau below 15K (evidenced by a smoother variation of the $\chi_M T$ value with temperaturte) at

values different than that expected for an S=0 or for any other possible multiplicity of the ground state. Additionally, the plateau tends to stabilize at a different $\chi_M T$ value for complexes **1** and **2**, although there is no apparent structural reason that justifies this magnetic divergence. A sudden increase of the susceptibility χ is observed at low temperatures in the χ versus T plot shown in Fig. 2.13.

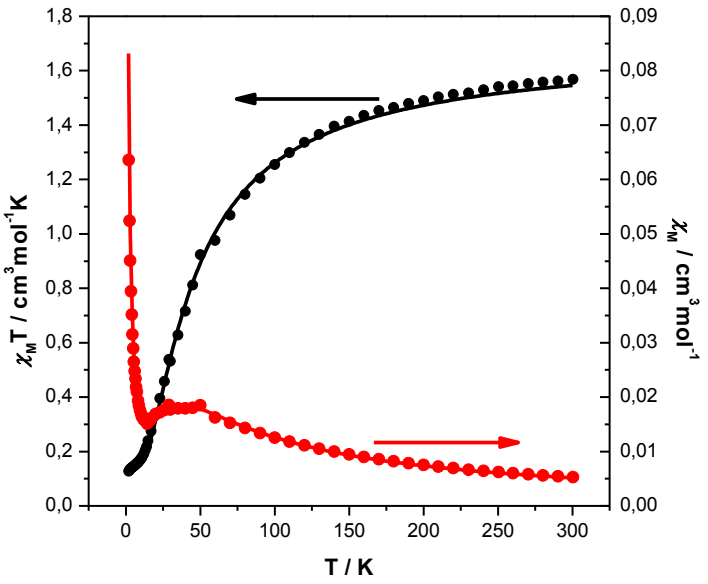

Fig. 2.13 Thermal dependence of the χ_M and $\chi_M T$ for complex **1**. The solid lines represent the simulation performed considering the magnetic model shown in Fig.12B for the Type B face-sharing dicubane structure characteristic of complexes **1** and **2**, using the parameters mentioned in the text. The presence of 15% impurities with an S ≠ 0 ground state was considered in the simulation.

This behaviour strongly suggests the presence of a significant amount of impurities with a spin different than 0, which are also responsible for the formation of the pseudo-plateau in the $\chi_M T$ versus T curves. By way of an example, the χ versus T and $\chi_M T$ versus T curves for complex **1**

could be successfully reproduced by adding 15% of impurities with an S = 1 ground state to the previous simulation. Temperature-independent paramagnetism (TIP) was considered equal to 200×10^{-6} cm^3 mol^{-1} for complex **1**. The experimental and simulated curves are shown in Fig. 2.13. The origin of the impurities can be hardly discussed since no structural evidence of their presence has been discerned. Cocrystallized ferromagnetic hydroxo-bridged Cu(II) complexes can be tentatively assigned as the responsible species. However, from a magnetic point of view, the presence of such impurities shows a strong effect on the low temperature range of the magnetic measurement, where the magnetic exchange between ions manifests the best. As a consequence the presence of impurities avoids a fine tuning of the value of the magnetic exchange in the cubane like compounds reported, even if based on structural parameters and previous magneto-structural correlations; the values obtained from the simulations seem fully reasonable considering the structures.

On the other hand, complex **3** presents a double-open cubane structure like the one in Fig. 2.12C. This structure is characterized by a Cu_4O_4 core where two Cu(II) ions adopt an octahedral environment (Cu1 and Cu2), while the other two adopt a square pyramidal geometry with a water molecule coordinated to the long axial position (Cu3 and Cu4).The Cu_4O_4 core possesses four short and two long Cu...Cu distances as a result of the particular relative arrangement of the axial axes and equatorial planes of the four Cu(II) ions, leading to a distorted [4+2] geometric type of cubane compounds proposed by Ruiz et al. [2.14c]. The corresponding equatorial or axial character of the bridging atoms with respect to the two connected Cu(II) ions in each pair is shown in Fig. 2.12C. Taking this structural arrangement in consideration and based on the same magneto-structural arguments discussed for complexes **1** and **2**, the magnetic behaviour of complex **3** can be explained using the model showed in Fig. 2.12D, where J_1 and J_2 are expected

to be weakly antiferromagnetic but significantly stronger than J_3, for which a null value can be reasonably assigned. Additionally, and considering the characteristic double-open cubane structure, the magnetic exchange coupling between Cu3 and Cu4 has been neglected since there is no direct magnetic superexchange pathway between this pair.

The $\chi_M T$ versus T curve for complex **3** starts from a value of 1.47 cm^3 K mol^{-1} at room temperature, in agreement with the value of 1.48 cm^3 K mol^{-1} expected for four uncoupled S = ½ spins assuming g = 2, and decreases continuously until 15 K where $\chi_M T$ stabilizes at a value of 0, evidencing the presence of an overall antiferromagnetic interaction and an S = 0 ground state. The magnetic behaviour of a double-open cubane structure like the one of complex **3** was simulated with the PHI program [2.39]. After considering the similarities in coordination geometry and bond lengths and angles, the model assumed the crystallographic equivalence of Cu1 and Cu2 on the one hand, and Cu3 and Cu4 on the other by assigning one single g value for each ion pair, i.e. $g_1 = g_2$ and $g_3 = g_4$. For the spin Hamiltonian $H = -J_1(S_1S_4+S_2S_3) - J_2(S_1S_3+S_2S_4) - J_3S_1S_2$, where $S_1 = S_2 = S_3 = S_4 = S_{Cu} = 1/2$, a good agreement between the experimental and simulated curves for **3** was found by using the following parameters: $g_1 = g_2 = 2.20$, $g_3 = g_4 = 2.18$, $J_1 = -36$ cm^{-1}, $J_2 = -44$ cm^{-1} and $J_3 = 0$ cm^{-1}. Temperature-independent paramagnetism (TIP) was considered equal to 200×10^{-6} cm^3 mol^{-1} for complex **3**. The simulated curve is represented together with the experimental values in Fig. 2.14. As experimentally suggested and theoretically anticipated, a weak antiferromagnetic coupling dominates the magnetic behaviour of complex **3**. The values obtained are in fair agreement with those observed in structurally similar compounds previously reported in the literature [2.36]. The nature and magnitude of J_i exchange constants in [4+2] cubane structures were studied by Tercero et al [2.14a]. The J_1 and J_2 coupling constants in complex **3** correspond to the four Cu-Cu pairs

connected at least through two short Cu-O bonds in the same exchange pathway (see Figs. 2.12C and 2.12D). In these cases, and according to the previously mentioned work, the sign of the coupling should be correlated with the Cu-O-Cu angle characteristic of these short exchange pathways. In the case of the Cu1-Cu4 and Cu2-Cu3 pairs, whose interaction is defined by J_1, Cu-O-Cu angles of ca. 106° are observed. On the other hand, the same angle shows values of ca. 118° for the Cu1-Cu3 and Cu2-Cu4 pairs, whose interaction is defined by J_2. Such values of the Cu-O-Cu angles are in agreement with the relative values of the magnetic exchange constants found experimentally, being J_1 slightly less antiferromagnetic than J_2; $|J_1|<|J_2|$.

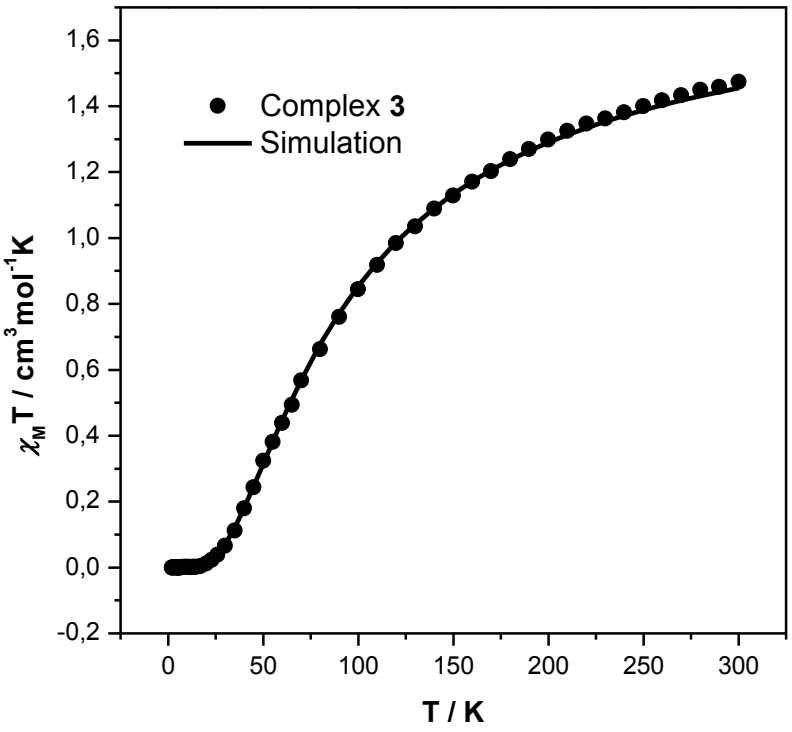

Fig. 2.14 Thermal dependence of the $\chi_M T$ for complex **3**. The solid line represents the simulation performed considering the magnetic model shown in Fig. 12D for the [4+2] double-open cubane structure characteristic of complex **3**, using the parameters mentioned in the text.

2.4 Conclusion

In summary, we report synthesis, crystal structures, and magnetic properties of tetranuclear [Cu_4] copper(II) complexes. Single crystal X-ray diffraction analysis evidenced the {Cu_4O_4} cubane core of the complexes. Both the complexes **1** and **2** have been synthesized using same Schiff base H_2L^1, but the use of different solvents results complexes **1** and **2** with different crystal system and space group. Complexes **1** and **2** possess face-sharing dicubane core structure, whereas use of slightly different Schiff base H_2L^2, gives complex **3** with double open cubane core structure. Weak π…π and C-H…π interactions result 2D supramolecular architectures of **1** and **2**. Variable temperature magnetic susceptibility measurements in the range 2 - 300 K indicate antiferromagnetic exchange coupling between copper centres in all complexes, in full agreement with the behaviour expected from their structural arrangement.